Modeling and Identification of Friction and Weight Forces on Linear Feed Axes as Part of a Disturbance Observer

Schöberlein Chris, André Sewohl, Holger Schlegel, and Martin Dix
Chemnitz University of Technology, Institute for Machine Tools and Production Processes, Chemnitz, Germany
Email: chris.schoeberlein@mb.tu-chemnitz.de, {andre.sewohl, holger.schlegel, martin.dix}@mb.tu-chemnitz.de

***Abstract*—Monitoring of production systems with special attention to the manufacturing processes is subject of intensive research efforts. Besides additional sensors close to the contact point between tool and workpiece, the pre-installed drive internal measuring systems of the feed axes offer a potential opportunity to access these forces. Due to their distance from the point of action, superimposed phenomena must be taken into account to achieve an appropriate estimation. In the case of linear feed axes, this applies in particular to prevailing frictional torques and forces. Depending on the structure of the feed axis, position- or workspace-dependent effects should also be considered. In addition, the influence of gravity becomes noticeable for vertical axes. In the context of this paper, suitable models and identification routines for both phenomena are developed and validated on a three-axis machine tool. Particular attention is devoted to an automated parameter identification as well as a compromise between model accuracy and the number of assignable parameters. Finally, all models are verified via exemplary air cutting and face milling experiments.**

***Index Terms*—production system, machine tool, linear feed axis, friction force, weight force, modelling, identification, disturbance observer**

I. Introduction

Monitoring of manufacturing processes is becoming increasingly important due to growing relevance of digitalization along the entire value chain. Particularly in metal-cutting production, monitoring of the process itself as well as the state of the tool can enhance productivity by avoiding unplanned downtimes and reducing scrap rates. Monitoring of the prevailing process forces using additional sensors on the tool or workpiece side is established in industry. On the other hand, it is desirable to use the already available internal drive signals of the machine tool for a superordinate process monitoring. For this purpose, there exist various observer approaches, which have already been classified and compared in [1]. In [2], a novel disturbance observer is presented based on the use of automatically identified models of the mechanical transmission function. Its fundamental structure is shown in Fig. 1. For the sake of simplicity, all forces are converted to equivalent torques.

In addition to the inverted transfer functions of the speed control system $G_p(s)$ and the mechanical transfer elements $G_{mech}(s)$, all superimposed force components must be modeled and subtracted from the measured motor current signal. This includes motor and load-side friction ($T_{f,m}$ and $T_{f,l}$) as well as potentially acting weight forces T_g. Therefore, suitable models and identification routines are required. In this context, the area of modeling and identification of tribological mechanisms on feed axes has been well developed on the research side. An overview of established models and a comparison with regard to their validity for different speed ranges is given in [3], [4].

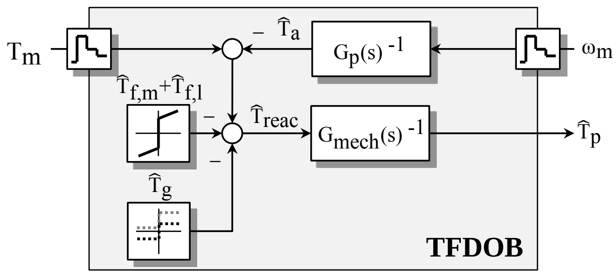

Figure 1. Transfer function-based disturbance observer (TFDOB) for drive-based disturbance estimation.

Considering the approaches with reference to the topic of drive-based process force estimation, the majority of the publications concentrate on static and speed-dependent friction models. This is justified by the relatively simple models and identification routines. Usually, an overall friction model is developed consisting of a coulomb and a viscous part like in [5], [6]. The friction parameters are identified by measuring the motor current of the axis at constant feed rates. Subsequently, the parameters are fitted by regression analysis [7] as well as utilizing a state observer [8] or kalman filter [9]. Jeong [10] goes one step further and differentiates the model equation based on the current feed rate. Therefore, the friction model is approximated using a polynomial approach for feed rates below 300 mm/min. In the case of higher velocities, again a linear relationship is applied. In addition, the Stribeck model is widely used, for example in [11] or [12]. All mentioned approaches are referred to

Manuscript received October 11, 2021; revised January 21, 2022.

doi: 10.18178/ijmerr.11.4.198-206

as static models, as they are only valid for areas with axis velocities significant greater than zero.

On the other hand, dynamic models are also widely addressed in research. The advantage of these models is that they also offer a description of the pre-sliding area at very low velocities. In addition, they are more accurate in areas of motion reversal. Jamaludin uses a Generalized Maxwell-slip friction model including a hysteresis function with non-local memory and frictional memory for the sliding regime as well as a Stribeck model for constant velocities [13]. Aslan designs a Kalman filter-based disturbance observer, which is supplemented by a Lund-Grenoble friction model [14]. In addition to Coulomb and Stribeck friction, hysteresis and presliding displacement are taken into account.

All mentioned approaches have in common that they do not consider any workspace-dependent friction influences. On the other hand, Yamada demonstrates in [15] and [16] that the friction behavior of linear feed axes with ball screw drives differs depending on the position in the working area. Although no basic approaches for modeling this effect are described in detail, the repeatability of the overall position-dependency is proven. Rudolph [17] shows in his publication that in the case of a combined fixed and loose bearing, the motor current required to overcome friction increases with the distance of the slide to the motor. Besides a speed-dependent part, he uses a logarithmic approach to approximate the position-dependent friction behaviour. Sato confirms the existence of a position-dependent friction part in [18] and approximates it with a polynomial model, which is not described in detail.

Overall, it can be stated that a substantial number of authors in the area of drive-based process force estimation deal with speed-dependent models. In addition, a non-negligible part of related publications focuses on the further development of dynamic friction models. Although these models provide good results in the microscopic range and for very low axis velocities, they are difficult to apply due to the large number of parameters and complex identification routines. Both approaches also have in common that their validity cannot be guaranteed in the entire workspace. Furthermore, the modeling of gravitational influence is often neglected due to the relatively simple relationships. In order to ensure broad industrial acceptance, automatic routines for axis weight correction are required, too.

Therefore, an automatic method for modeling the speed and position-dependent friction behavior as well as the influence of gravity on linear feed axes is presented in the context of this paper. It is organized as follows. Section two presents the basic structure of a linear feed axis including the underlying equilibrium of forces. Section three is initially devoted to the systematics for modeling and identifying the friction models on linear feed axes. Subsequently, the correction value for the motor current caused by the gravitational influence on vertical feed axes is identified. That is based on the already recorded frictional force curves. Eventually, all models are verified on an exemplary three-axis machining center through exemplary air cutting and face milling experiments. The paper closes with a summary of the results and an outlook on future research goals.

II. Structure of Linear Feed Axes

The basic structure of a linear electromechanical feed axis, as it is typically used in modern production systems, is illustrated in Fig. 2. It consists of an electrical part including an industrial control, a converter system with servomotor and the associated position measuring systems, as well as a mechanical part. In the case of linear feed axes, the latter is usually designed as a ball screw drive with corresponding coupling, bearing and gear elements. In some cases, additional elements like a coverage for the working area are part of the mechanical system. The process forces F_p usually act on the load side of the feed axis.

Starting point of the considerations is the equilibrium of forces. For the sake of simplicity, all forces are reduced onto the motor shaft as effective torques. The motor torque is calculated as product of the torque constant K_m and the motor current I_m and is equivalent to the sum of acceleration torque T_a and applied load torque T_l.

$$T_m = I_m * K_m = T_a + T_l \tag{1}$$

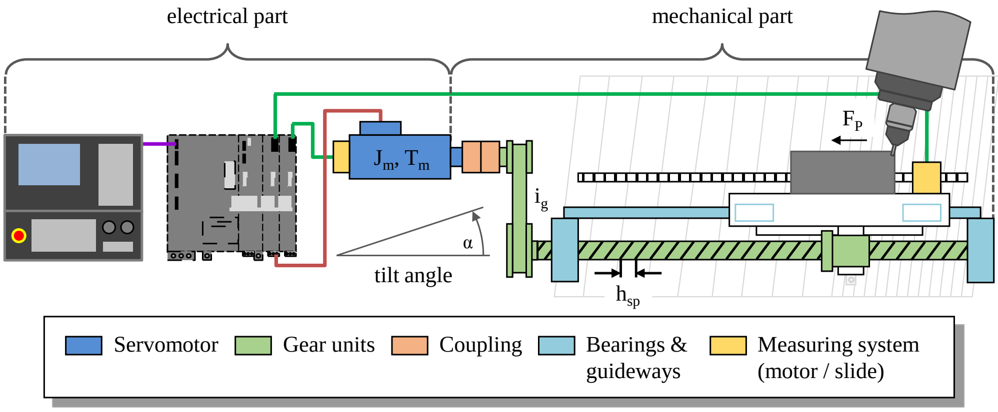

Figure 2. Structure of a linear electromechanical feed axis.

While the acceleration torque depends on the current axis acceleration and the total moment of inertia, the load torque consists of several parts. In addition to the repercussions of the

machining process T_p in feed direction, the sum of all friction torques T_f and, depending on the axis alignment, the weight torque T_g are included.

$$T_l = T_p + T_f + T_g \qquad (2)$$

The required torque to overcome the weight forces acting on the axis (3) is ultimately dependent on the gravitational constant g, the moving masses in the drive train m_{tot}, the tilt angle of the axis α, the spindle pitch h_{sp}, potential gear ratios i_g and the overall efficiency of all transmission elements η_{tot}.

$$T_g = h_{sp} * m_{tot} * g * \sin(\alpha) / (2\pi * i_g * \eta_{tot}) \qquad (3)$$

In contrast, the frictional part of the load torque is calculated as the sum of various individual parts.

$$T_f = (T_{f,g} + T_{f,c} + T_{f,b}) / (2\pi * i_g * \eta_g) \qquad (4)$$

This includes the friction in the guideways $T_{f,g}$ and spindle bearings $T_{f,b}$ as well as frictional torques caused by covers $T_{f,c}$ installed in the working area. The transmission ratio and its efficiency η_g must also be taken into account. For a detailed description of the individual parts and further parameters see [19]. Since an individual modeling of the friction parts is not achievable without dismantling components of the mechanical structure, an overall friction model is considered in the next section.

III. Identification of Friction Model and Weight Force Correction

This section describes the general procedure for the automatic generation of the friction models as well as the identification of the weight force correction value. All examinations were carried out on the three-axis machining center from DMG Mori shown in Fig. 3.

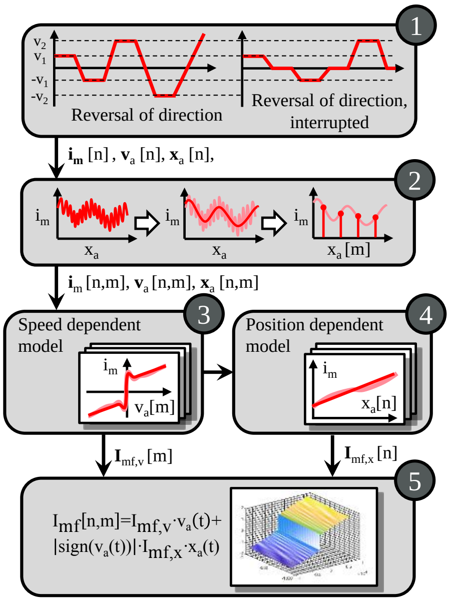

Figure 3. Methodology for determining workspace-dependent friction model for linear feed axes.

A. Friction Model

As already described in the previous section, the friction conditions cannot easily be mapped in detail and separately for each part of the mechanical system. For this reason, an overall friction model of the feed axis is developed, which is divided into a speed-related and a position-related part. The complete process for determining the model is illustrated in Fig 4. In the first step, the respective axis is moved at constant feed rate over the entire travel path with the illustrated speed profiles. At the same time, the motor current i_m, feed rate v_a and axis position x_a are recorded using the control-internal measuring function. This is repeated three times for each of the speed levels shown in Table I.

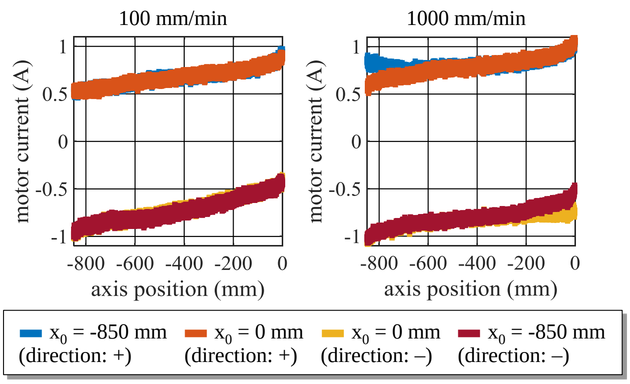

Figure 4. Motor current at constant feed rates depending on the axis position.

TABLE I. Feed Rate Levels

Designation	v_a in mm/min	$v_{a,n}$ in mm/min
Level 1	10 … 90	10
Level 2	100 … 900	100
Level 3	1000 … 9000	1000

Since there are no effective external forces or accelerations on horizontal axes, with the exception of the start, end and reversal points, the measured motor current is used exclusively to overcome the frictional forces. For vertical axes an additional correction of the axis weight is necessary, which is described in the next subsection. Fig. 5 shows exemplary motor current signals for two constant feed rates over the entire travel range of the x-axis. Additional, a distinction is made between the direction and the course of movement, i.e. with or without interrupted reversal of direction. It becomes clear that the motor current depends on the position of the axis. Furthermore, the signal characteristics for both directions are very similar. With regard to the course of movement, however, differences can be determined according to the feed rate. For lower feed rates (Fig. 5, left) the course of the motor current is independent of the starting point of the axis motion. In contrast, there occur some differences for higher feed rates (Fig. 5, right). In particular, in the first movement segment of the interrupted movement reversal, the motor current is not equal to the continuous motion.

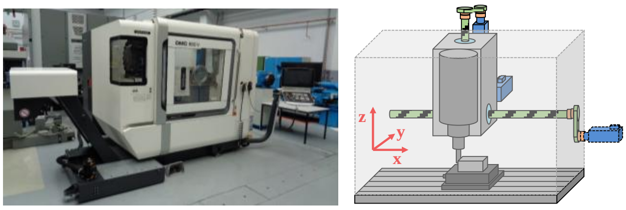

Figure 5. Three-axis machining center DMC 850 V (DMG Mori).

In step two, all three recorded friction fields are averaged and the signals are filtered with a sliding average filter. To reduce the modeling effort, the signal values are also divided into m position segments depending on the spindle pitch h_{sp} (5)

$$m = h_{sp} / 3 \tag{5}$$

In a third step, these m signal profiles are used as input signals for estimating the speed-dependent friction model. The already presented approach in [2] contains of four parts (coulomb, exponential, logarithmic, linear) with overall seven unknown parameters $P_{v,1}$ to $P_{v,7}$ and depends solely on the axis velocity v_a according to (6) to (10).

$$I_{mf,v}\ (v_a) = sign(v_a) * (I_{f,c} + I_{f,exp} + I_{f,log}) + I_{c,lin} \tag{6}$$

$$I_{f,c}\ (v_a) = P_{v,1} \tag{7}$$

$$I_{f,exp}\ (v_a) = (P_{v,2} - P_{v,1}) * exp(-|v_a / P_{v,3}|, P_{v,4}) \tag{8}$$

$$I_{f,log}\ (v_a) = P_{v,5} * ln(|v_a| / P_{v,6} + 1) \tag{9}$$

$$I_{f,lin}\ (v_a) = P_{v,7} * v_a \tag{10}$$

The model parameters are approximated by minimizing the square error between the measured and modeled motor current. The examinations have shown that separate estimations for positive and negative feed rates lead to a significant increase in model quality. As result of this module, a speed-dependent friction current signal Imf,v is obtained for each of the m positions. These signals serve as input of step four and form the basis for estimating the position-dependent friction behavior. Therefore, different model approaches were examined, whereby a linear model approach according to (11) offers a good compromise between the number of parameters and the accuracy of the model. Analogous to the speed-dependent part, the square error between measured and modeled motor current $I_{qf,x}$ is minimized for all axis velocity segments.

$$I_{mf,x}\ (x) = (P_{x,1} + P_{x,2} * x_a) \tag{11}$$

In the last step, the parameters of both models are averaged for each direction of movement. The mean value of these parameter sets ultimately provides the final parameters of the speed- and position-dependent friction model. Note that in some cases it could be beneficial to use separate position models for positive and negative direction of movement. For example, Rudolph [17] determined a rise in the motor current with increasing distance between axis slide and motor. A similar effect can be observed in the model validation in section four. However, due to the minor impact on the accuracy, this effect is not considered further. Eventually, the complete friction model is calculated as the sum of both model equations. The signum function in (12) ensures that the position-dependent part is only effective during a motion of the axis.

$$I_{mf}\ (v_a, x_a) = I_{mf,v} * v_a(t) + |sign(v_a(t))| * I_{mf,x} * x_a(t) \tag{12}$$

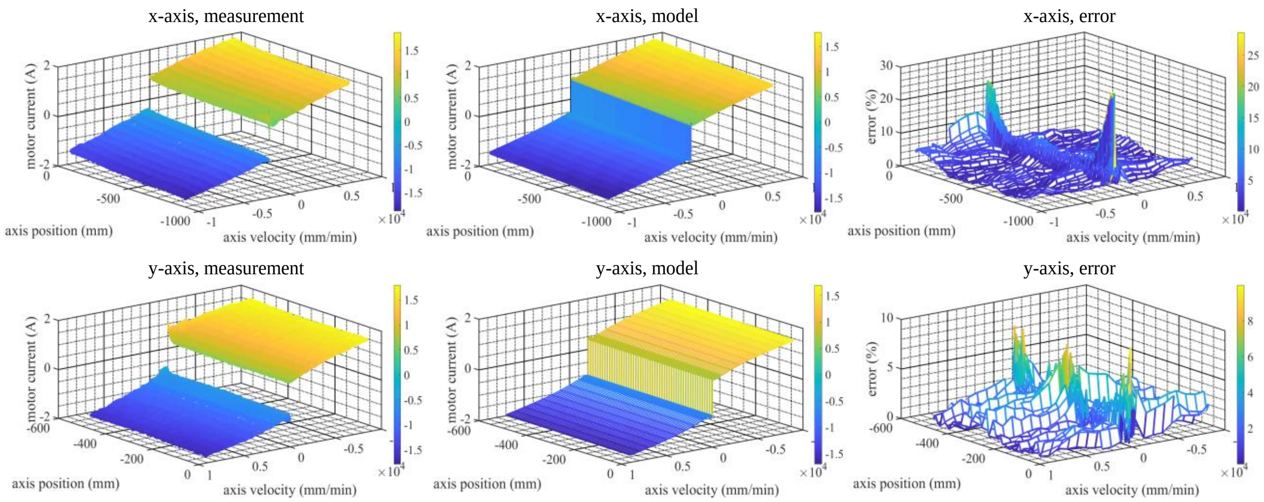

Figure 6. Measured (left), modeled (center) and error (right) friction fields of x- and y-axis.

Fig. 6 shows the measured and estimated friction fields as well as the modeling error for the x- and y-axes. Except the edge areas, there is good agreement between the measurement and the model. The errors arise on the one hand from acceleration currents at the start and reversal points, but also from the already discussed differences in the motion. Furthermore, deviations become more apparent for low axis velocities. Nonetheless, the mean error between model and measurement for the entire speed and travel range is only 3.2 % for the x-axis and 2.4 % for the y-axis.

As can be seen from the estimated parameters in Table II, the position-dependent friction component is more significant in case of the x-axis. This is justified by the different types of workspace coverage. While the x-axis has a large fold coverage, the separation of y- and z-axes from the work area is realized by a scraper. The variations in the current signal depend on the direction of movement and axis position, since the folds are pushed into one another to different degrees according to their position. The extent to which the determined models are also valid for a more complex sequence of axis motions is examined in section four. Regarding the z-axis, the measured motor current signals still have to be corrected for the weight force. However, the final parameters are already included in Table II.

TABLE II. IDENTIFIED FRICTION PARAMETERS

Parameter	Identified friction values		
	x-axis	*y-axis*	*z-axis*
$P_{v,1}$	-0.767	-0.845	-0.897
$P_{v,2}$	7.564	-3.680	-1.493
$P_{v,3}$	3.357	-0.537	0.537
$P_{v,4}$	0.034	-0.558	0.019
$P_{v,5}$	11.572	40.328	1.925
$P_{v,6}$	0.241	-0.433	0.675
$P_{v,7}$	1.029	1.820	5.072
$P_{x,1}$	0.141	-0.047	-0.059
$P_{x,2}$	3.375	-1.758	-2.244

B. Axis Weight Correction

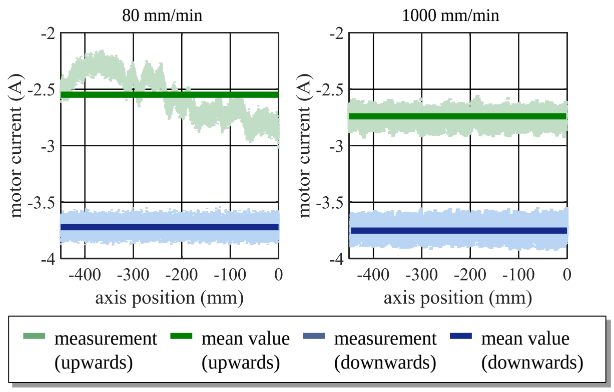

Figure 7. Measured and averaged current curves for 80 mm/min (left) and 1000 mm/min (right) of the z-axis.

The developed approach for identifying the proportion of weight force in the motor current of the vertical axis is shown in Fig. 7. It is initially assumed that the motor torque for each direction is applied completely to overcome the friction and gravitational effects. As before, this assumption is permissible due to the constant feed rates. The steps one and two with asterisk are optional, as the required signals have already been recorded as part of the friction measurements. In the case of the averaged and segmented signals, it is assumed that there are no major differences for both directions of motion. In the third step, the current signals are averaged separately for each of the n speed levels and both directions (upwards $i_{mg,u}$ and downwards $i_{mg,d}$) in order to eliminate the influence of the axis position. The current signals for two exemplary speed levels are shown in Fig. 8. In case of downwards motion and an axis feed rate of 100 mm/min, the motor current is not constant across the axis position. One possible cause are stick-slip effects, as the effect cannot be observed for higher axis velocities (e.g. Fig. 8, right). In order to avoid errors in the calculation of the gravitational influence, all velocities with similar effects are excluded. For the considered machine axis, this corresponds to all axis velocities less than 500 mm/min. In step four, a final averaging of all averaged current signals takes place. As a result, the weight correction current calculates to I_{mg} = 3.234 amperes. Fig. 9 shows that by offsetting this value, an adequate correction of the gravitational influence of the vertical axis is achieved. In combination with the calculated friction model, the average error between measurement and model calculates to approximately 10 % over the entire travel range and all velocity levels. The reason for the increased model deviations compared to the x- and y-axes is the stick-slip behavior in the range of low speeds (cf. Fig. 8). The identified friction parameters are shown in Table II.

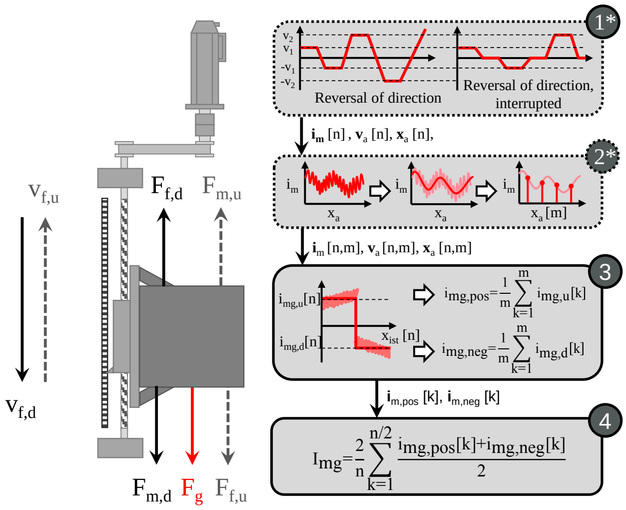

Figure 8. Methodology for determining weight force correction value on vertical linear feed axes.

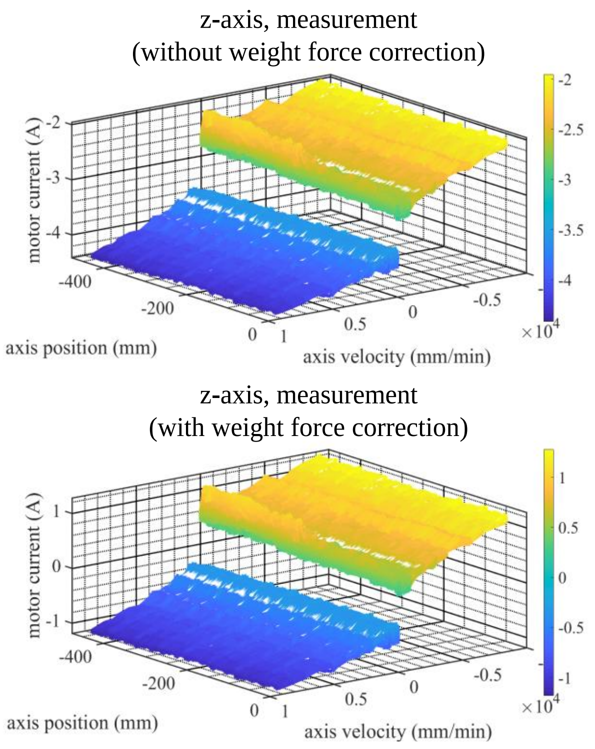

Figure 9. Measured friction field of the z-axis without (upper) and with (lower) weight force correction.

IV. Validation

After the friction models for all three axes and the weight correction of the vertical z-axis have been calculated, all models are validated using an exemplary machining contour. Its shape, shown in Fig. 10, is based on the contour specified in [20] for assessing the positioning accuracy of production systems. The experiments were carried out at different tilt angles in the working area and at different feed rates. At the same time, the motor currents as well as positions and velocities of the axes were recorded. Afterwards, the frictional forces were calculated as a function of the recorded signals.

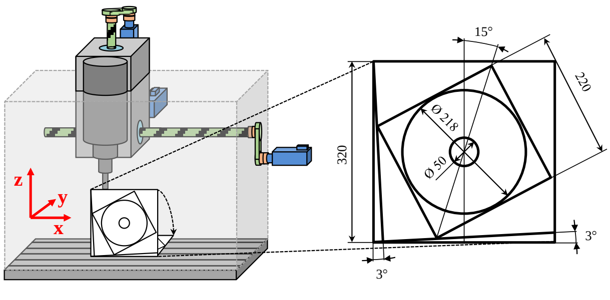

Figure 10. Measured friction field of the z-axis without (upper) and with (lower) weight force correction.

Fig. 11 illustrates two exemplary cases. The left diagrams show the measured axis positions and motor currents as well as the associated friction estimations in the x-y-plane. The feed rate is set to 500 mm/min. The diagrams on the right show the same measured and modeled signals, but for a motion in the x-z-plane with a programmed feed rate of 1000 mm/min. In addition to the estimated overall friction model, the speed and position-related parts are plotted individually. Except for the modeled acceleration phases, a good correspondence between model and measurement can be determined for all axes. Only in the first part of the movement sequence arise clear differences for two movement segments of the x- and y-axes. This phenomenon is illustrated for the motor current signal of the x-axis in the range of approx. 40 to 80 seconds. As it can be seen in the target contour and the measured position profile, no feed rate is programmed for the x-axis in this movement segment. Hence, only the y-axis should move. However, when considering the actual feed rate of the x-axis, a value in the range of less than one mm/min could be detected. This already shows the limits of the utilized model approach, which cannot provide an appropriate approximation for movements in the range of very low feed rates. Therefore, an additional dynamic friction model is required. A comparison for the range of motion for the x-z plane shows that the mentioned effect does not occur. The minor deviations are caused by the current controller and its remaining integration value. On the other hand, comparing the modeled friction curves for all three axes, the advantage of the position-dependent friction model is apparent solely for the x-axis. Nonetheless, the correction of the weight forces for the z-axis is of particular importance. It is also recognizable that the overall model for downward motion (lower absolute motor currents) is slightly closer to the measured current curves. However, it can be stated that the friction models for all cases and axes tend to be overestimated. Nonetheless, for the example contours and considering various programmed feed rates (200 mm/min, 500 mm/min, 1000 mm/min, 5000 mm/min), the absolute mean error between model and measurement is always lower than 15 %. Possible reasons were already observed when measuring the initial friction curves. In this case, differences of +/– 10 % over all three measurement runs occurred. In addition, the temperature of the lubricant of the guideways has a significant influence on the friction behavior and therefore on the motor current under constant axis movement. In case of the x-axis, this fact is shown exemplary in Fig. 12.

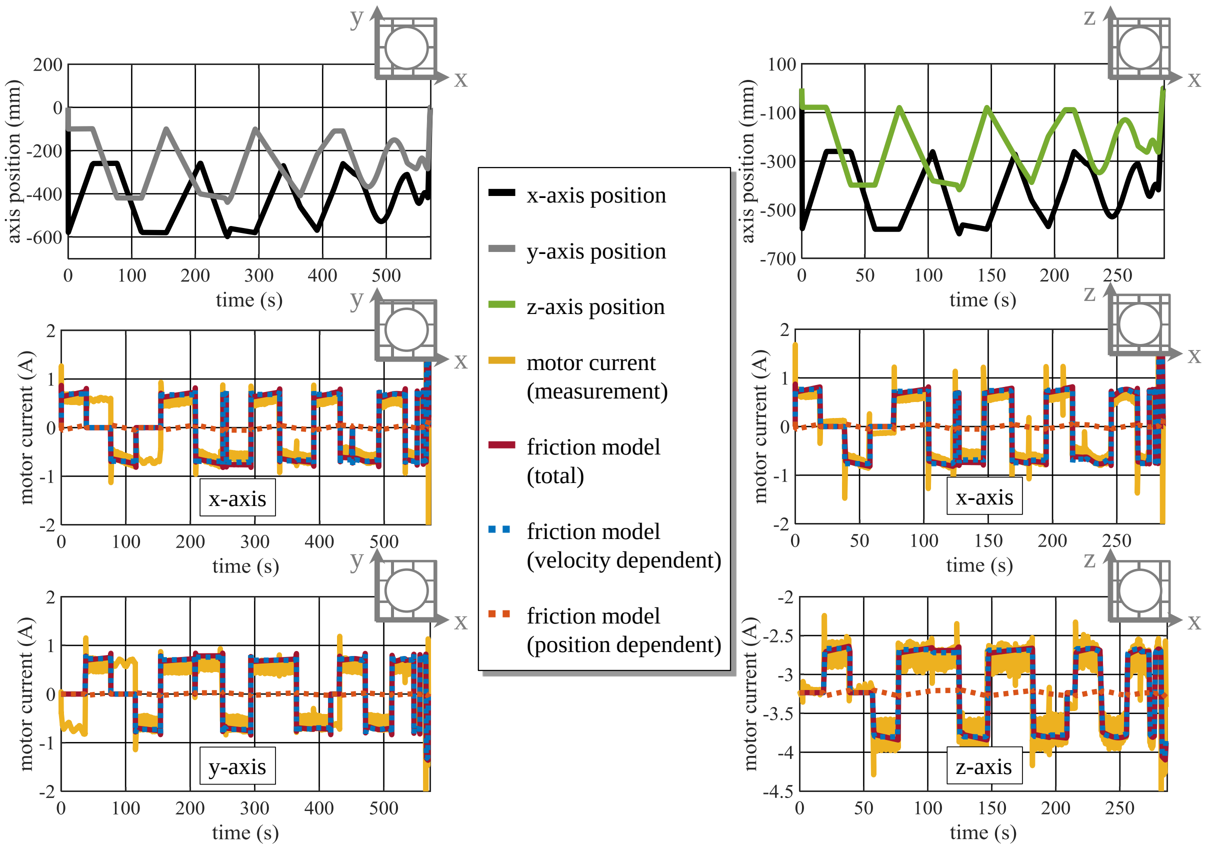

Figure 11. Axis positions and motor currents under selected machining contour in air cutting.

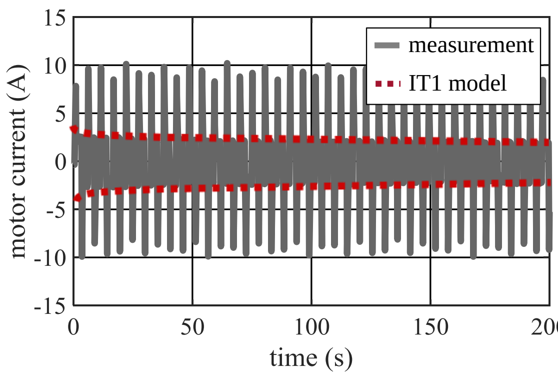

Figure 12. Motor current of the x-axis under cyclical traversing movement with 10000 mm/min.

The axis was moved over several cycles in the entire travel range and the motor current was recorded. The programmed feed rate is set to 10000 mm/min. A continuous drop in the motor current signal can be observed after just a few motion cycles. This influence becomes less significant as the temperature of the lubricant increases further. A reduction in the measured motor current of 5–10 % can be seen after just 10 seconds or two motion cycles, and of 15–20 % after 50 seconds or 10 cycles. Overall, this behavior can be approximated with an IT1 model. However, since the temperature value of the lubricant is usually not available in the machine control, it cannot be incorporated into the developed model. In order to take this influence into account, a warm-up phase could be provided before each machining. At the same time, a cyclical update of the friction model can contribute to increase its accuracy.

Eventually, the developed models should be incorporated as part of a disturbance observer for drive-based process force estimation (cf. Fig. 1). Hence, their suitability must also be evaluated under process conditions. In Fig. 13, the applied tool path and workpiece are shown as well as the measured position and motor current for the x- and y-axes. In addition to the individual parts of the friction model, the filtered motor current is plotted. The tool is a 3-flute face milling cutter with a diameter D = 25 mm, the workpiece material is C45 steel. The depth of cut was set to ae = 3 mm The programmed values for feed rate and spindle speed were 765 mm/min and 2548 min-1, respectively.

For both axes a clear distinction can be made between the proportions of friction and process forces in the motor current signal. In particular, the deviations of the y-axis correspond to the expectations from the air cutting experiments. On the other hand, the estimations for the x-axis are more accurate for negative motion direction, especially when combining velocity- and position-dependent friction models. Due to the low process-related signal amplitudes in the case of positive direction of motion, a separation between friction and process forces is only possible to a limited extent. For valid statements, however, further experiments under process conditions are necessary.

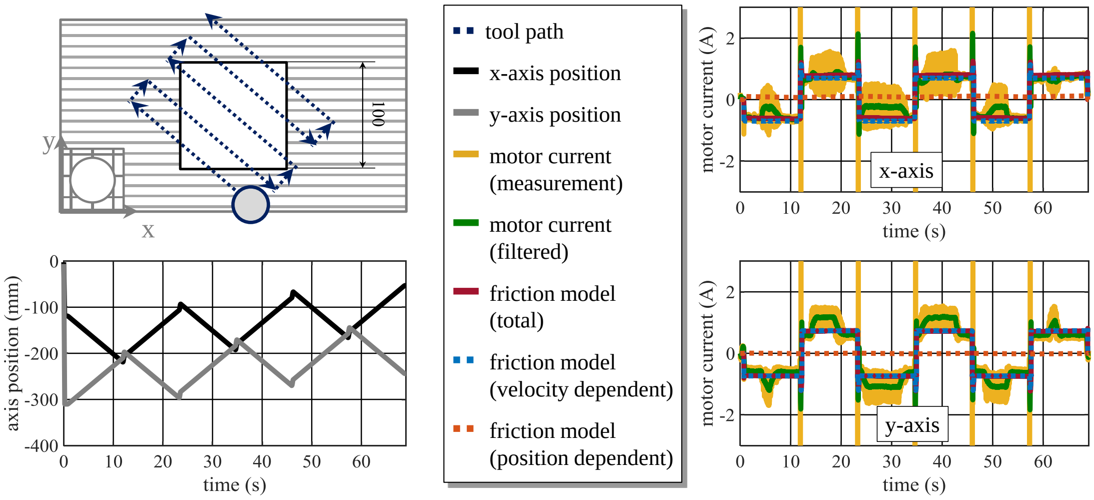

Figure 13. Tool path, axis positions and motor currents under an exemplary machining process.

V. Conclusion

In this paper, a method for automatic identification and modeling of friction and gravitational influences on linear feed axes was presented and examined on a three-axis machining center. Based on the equilibrium of forces, an automated approach was developed to determine speed- and position-dependent friction models for each horizontal axis as well as the correction current for the weight forces of the vertical axis. The comparison of measured and modeled friction fields showed a high degree of agreement. The mean deviations for the horizontal axes are in the lower single-digit percentage range. These errors are caused by the acceleration parts at the motion starting points and from differences in the first third of the interrupted movement profiles. The slightly increased model deviations in the case of the vertical z-axis arise from noticeable stick-slip behavior in the case of low feed rates, especially when traveling downwards. During the subsequent validation of the models using a standardized sample contour, the high quality of the models was demonstrated. Especially, the value of the position-dependent model was particularly proven for the x-axis, caused by its fold coverage. Overall, however, the modeled motor current is estimated 10-15 % too high. In addition to basic model inaccuracies, the main reason is the dependence of the frictional force on the temperature of the lubricant of the guideways. Furthermore, motion segments with micro-movements and feed rates of less than one mm/min are not incorporated in the model. Eventually, the friction models were examined under real process conditions using a face milling process. Here, the high quality of the estimated friction models could also be confirmed.

Future activities should focus on expanding the friction models in terms of a dynamic component. This could contribute to an increasing model quality, particularly in the case of interrupted movements and changes in direction as well as low feed rates. In addition, further superimposed influences must be taken into account to applicate the disturbance observer presented in Fig. 1. In particular, the correction of the acceleration and standstill phases as well as the mechanical transmission behavior are important examples. With regard to the correction of the axis weight, the system should be generalized regarding rotary axes. Especially in the case of pivot units, additional position-related and possibly mass-related effects occur.

Conflict of Interest

The authors declare no potential conflict of interest relevant to this article.

Author Contributions

Chris Schöberlein conducted the research, carried out the experiments, analyzed the data and wrote the paper; André Sewohl edited the paper; Holger Schlegel edited the paper and supervised the fundamentals of the research; Martin Dix edited the paper and supervised the project; all authors had approved the final version;

Acknowledgment

ZIM Zentrales Innovationsprogramm Mittelstand
Supported by: Federal Ministry for Economic Affairs and Energy
on the basis of a decision by the German Bundestag

Funded by the Federal German Ministry for Economic Affairs and Energy

References

[1] C. Schoeberlein, M. Norberger, H. Schlegel, and M. Putz, "Simulation and disturbance estimation of speed-controlled mechatronic drive systems," *MATEC Web of Conferences*, vol. 306, 2020

[2] C. Schoeberlein, A. Schleinitz, H. Schlegel, and M. Putz, "Simulative investigation of transfer function-based disturbance observer for disturbance estimation on electromechanical axes," in *Proc. the 17th Int. Conf. on Informatics in Control, Automation and Robotics*, 2020, pp. 651–658.

[3] T. Tjahjowidodo, F. Al-Bender, H. Van Brussel, and W. Symens, "Friction characterization and compensation in electro-mechanical systems," *J. of Sound and Vibration*, vol. 308, pp. 632–646, 2007.

[4] M. Schwenzer, T. Auerbach, K. Miura, B. Döbbeler, and T. Bergs, "Support vector regression to correct motor current of machine tool drives," *J. of Intelligent Manufacturing*, vol. 31, pp. 553–560, 2019.

[5] R. Sato, M. Hasegawa, and K. Shirase, "Cutting force monitoring based on frequency analysis of feed motor torques," *J. of SME Japan*, 2013.

[6] R. Koike, Y. Kakinuma, and T. Aoyama, "Drill fracture detection by integrating disturbance observer and rotational digital filter," *CIRP J. of Manufacturing Science and Technology*, vol. 7, pp. 177–184, 2014.

[7] X. Li, R. Du, B. Denkena, and J. Imiela, "Tool breakage monitoring using motor current signals for machine tools with lienar motors," *IEEE Transactions on Industrial Electronics*, vol. 52, no. 5, pp. 1403–1408, 2005.

[8] S. Katsura, J. Suzuki, and K. Ohnishi, "Pushing operation by flexible manipulator taking environmental information into account," *IEEE Transactions on Industrial Electronics*, vol. 53, no. 5, pp. 1688–1697, 2006.

[9] T. Kim, J. Woo, D. Shin, and J. Kim, "Indirect cutting force measurement in multi-axis simultaneous NC milling processes," *International J. of Machine Tools and Manufacture*, vol. 39, pp. 1717–1731, 1999.

[10] Y. Jeong and D. Cho, "Estimating cutting force from rotating and stationary feed motor currents on a milling machine," *International J. of Machine Tools and Manufacture*, vol. 42, pp. 1559–1566, 2002.

[11] S. Yamato and Y. Kakinuma, "Precompensation of machine dynamics for cutting force estimation based on disturbance observer," *CIRP Annals–Manufacturing Technology*, vol. 69, pp. 333–336, 2020.

[12] B. Denkena, B. Bergmann, and D. Stoppel, "Reconstruction of process forces in a five-Axis milling center with a LSTM neural network in comparison to a model-based approach," *J. of Manufacturing and Materials Processes*, vol. 4, no. 62, 2020.

[13] Z. Jamaludin, H. Van Brussel, G. Pipeleers, and J. Swevers, "Accurate motion control of xy high-speed linear drives using friction model feedforward and cutting forces estimation," *CIRP Annals–Manufacturing Technology*, vol. 57, pp. 403–406, 2008.

[14] D. Aslan and Y. Altintas, "Prediction of cutting forces in five-axis milling using feed drive current measurements," *IEEE/ASME Transactions on Mechatronics*, vol. 23, no. 2, pp. 833–844, 2018.

[15] Y. Yamada and Y. Kakinuma, "Sensorless cutting force estimation for full-closed controlled ball-screw-driven stage," *International J. of Advanced Manufacturing Technology*, vol. 87, pp. 3337–3348, 2016.

[16] Y. Yamada, S. Yamato, and Y. Kakinuma, "Mode decoupled and sensorless cutting force monitoring based on multi-encoder," *International J. of Advanced Manufacturing Technology*, vol. 92, pp. 4081–4093, 2017.

[17] C. Brecher and T. Rudoplph, "In process identification of cutting condition using digital drive signals," in *Proc. the CIRP 2nd International Conference Process Machine Interactions*, 2010.

[18] T. Sato, S. Yamato, Y. Imabeppu, N. Irino, and Y. Kakinuma, "Precise cutting force estimation by hybrid estimation of DC/AC components," in *Proc. the ASME 2020 International Symposium on Flexible Automation*, 2020.

[19] H. Groß, J. Hamann, and G. Wiegärtner, "Electrical drive systems in automation technology: basics, calculation, design," Erlangen, Publicis Corporate Publishing, 2006. (only in german)

[20] ISO 10791-7:1998-02-15, *Test Conditions for Machining Centres – Part 7: Accuracy of a Finished Test Piece*, 1998.

Schöberlein Chris was born in 1987. He received B. Sc. Degree in Microtechnology/Mechatronics in 2014 (Chemnitz University of Technology). And he obtained M. Sc. Degree in Microtechnology/Mechatronics in 2016 (Chemnitz University of Technology). Currently, he is working as a research associate at Chemnitz University of Technology, Professorship for Production Systems and Processes (Institute of Machine Tools and Production Systems), Department Control and Control Feedback technology. His research interests include Control theory, Control Strategies for mechatronic drive systems, Monitoring and Identification of electromechanical axes, Process monitoring on machine tools based on machine internal data

.